Molecular Biology of the Cell
Vol. 17, 5324–5336, December 2006

Ubc9 Regulates Mitosis and Cell Survival during Zebrafish Development[D]

Matthias Nowak* and Matthias Hammerschmidt

Georges Köhler Laboratory, Max-Planck Institute of Immunobiology, 79108 Freiburg, Germany

Submitted May 11, 2006; Revised September 21, 2006; Accepted October 4, 2006
Monitoring Editor: Marianne Bronner-Fraser

Many proteins are modified by conjugation with Sumo, a gene-encoded, ubiquitin-related peptide, which is transferred to its target proteins via an enzymatic cascade. A central component of this cascade is the E2-conjugating enzyme Ubc9, which is highly conserved across species. Loss-of-function studies in yeast, nematode, fruit fly, and mouse blastocystes point to multiple roles of Ubc9 during cell cycle regulation, maintenance of nuclear architecture, chromosome segregation, and viability. Here we show that in zebrafish embryos, reduction of Ubc9 activity by expression of a dominant negative version causes widespread apoptosis, similar to the effect described in *Ubc9*-deficient mice. However, antisense-based knock down of zygotic *ubc9* leads to much more specific defects in late proliferating tissues, such as cranial cartilage and eyes. Affected cartilaginous elements are of relatively normal size and shape, but consist of fewer and larger cells. Stainings with mitotic markers and 5-Bromo-2′-deoxyuridine incorporation studies indicate that fewer chondrocyte precursors are in mitosis, whereas the proportion of cells in S-phase is unaltered. Consistently, FACS analyses reveal an increase in the number of cells with a DNA content of 4n or even 8n. Our data indicate an in vivo requirement of Ubc9 for G2/M transition and/or progression through mitosis during vertebrate organogenesis. Failed mitosis in the absence of Ubc9 is not necessarily coupled with cell death. Rather, cells can continue to replicate their DNA, grow to a larger size, and finish their normal developmental program.

INTRODUCTION

Posttranslational modifications of proteins have a strong impact on protein function, localization, and/or stability. Ubiquitin and the small ubiquitin-like modifier (Sumo) are gene-encoded peptides that are conjugated to target proteins via a cascade of enzymatic reactions (Weissman, 2001; Schmidt and Muller, 2003). After processing from a precursor protein, the C-termini of ubiquitin or Sumo are activated by an E1 enzyme and covalently bound to an E2-conjugating enzymes, followed by the E3 ligase-catalyzed transfer to the substrate protein. In contrast to ubiquitination, sumoylation appears to be mediated by a single E2-conjugating enzyme named Ubc9, which binds directly to all thus far examined sumoylated proteins (Desterro *et al.*, 1997; Gong *et al.*, 1997; Johnson and Blobel, 1997). The existence of Sumo-specific E3 ligases has long been subject to controversies (Seeler and Dejean, 2003); however, recently a number of proteins were shown to have Sumo E3 activity (Johnson and Gupta, 2001; Pichler *et al.*, 2002; Kagey *et al.*, 2003).

The molecular effects caused by protein sumoylation are diverse, affecting different protein properties and cellular processes. Thus, for some target proteins sumoylation regulates their nucleo-cytoplasmic trafficking (Matunis *et al.*, 1996; Epps and Tanda, 1998) and subnuclear localization. In particular, the formation of PML (promyelocytic leukemia) nuclear bodies (Muller *et al.*, 1998), and the inactivation of several transcriptional activators like Lef-1 (Sachdev *et al.*, 2001) and Sp3 (Ross *et al.*, 2002; Sapetschnig *et al.*, 2002) via a recruitment to these nuclear compartments have been shown to be sumoylation-dependent (reviewed in Gill, 2003). In addition, protein sumoylation is involved in the regulation of DNA repair (Hardeland *et al.*, 2002; Hoege *et al.*, 2002; Stelter and Ulrich, 2003) and is required for proper chromosome condensation and separation (Hari *et al.*, 2001; Strunnikov *et al.*, 2001; Bachant *et al.*, 2002; Azuma *et al.*, 2003).

However, the broader impact of sumoylation on entire cellular systems, and the degree of conservation of this impact between different organisms, is less well understood. In budding yeast (*Saccharomyces cerevisiae*), Ubc9 deficiency is lethal, whereas analyses with a temperature-sensitive allele indicate that Ubc9 is required for progression through mitosis, mediating degradation of mitotic cyclins (Seufert *et al.*, 1995). In contrary, Ubc9 (Hus5) mutants in fission yeast (*Schizosaccharomyces pombe*) are viable, but display defects during chromosome segregation and reduced cellular growth (al-Khodairy *et al.*, 1995), similar to the defects of mutants in the Sumo gene (Tanaka *et al.*, 1999). RNAi-mediated knockdown of Ubc9 in the nematode *Caenorhabditis elegans* results in several specific developmental defects that resemble phenotypes produced by mutations in known developmental regulators such as Hox genes (Jones *et al.*, 2002). Similarly, in the fruit fly *Drosophila melanogaster*, loss of Ubc9 in the *semushi* mutant causes patterning defects associated with the misregulation of the anterior-posterior morphogen bicoid (Epps and Tanda, 1998). Together these studies indicate that in addition to the regulation of particular cellular processes, Ubc9 can influence developmental programs of higher multicellular organisms, accounting for spatial pat-

This article was published online ahead of print in *MBC in Press* (http://www.molbiolcell.org/cgi/doi/10.1091/mbc.E06–05–0413) on October 11, 2006.

[D] The online version of this article contains supplemental material at *MBC Online* (http://www.molbiolcell.org).

* Present address: Biotechnology Centre, University of Technology Dresden, Am Tatzberg 47–49, 01307 Dresden, Germany.

Address correspondence to: Matthias Hammerschmidt (hammerschmid@immunbio.mpg.de).

tern formation and differential cell specification. However, the connection between these developmental roles of Ubc9 and its basic functions during cell cycle and cell growth regulation remained elusive. In vertebrates, the impact of sumoylation on developmental programs is even less clear. Inducible loss of Ubc9 function in a chick cell line leads to polynucleated cells and cell cycle–independent apoptosis (Hayashi *et al.*, 2002), whereas in mouse embryos, loss of Ubc9 causes chromosome mis-segregation and loss of nuclear integrity (Nacerddine *et al.*, 2005). These defects result in early lethality of mutant embryos, preventing analyses to address possible roles of Ubc9 during later developmental processes.

Here we investigate the function of Ubc9 during zebrafish development. Similarly to the phenotype observed in mutant mice, expression of a dominant negative version of Ubc9 leads to early embryonic apoptosis. In contrast, because of compensation by maternally supplied Ubc9 protein, inactivation of zygotic Ubc9 function by injection of antisense morpholino oligonucleotides causes later and more specific developmental defects in brain, eyes, and pharyngeal arches. In the arches of *ubc9.1* morphant embryos, cells seem to bypass mitosis and continue to grow, leading to normal-sized cartilaginous elements consisting of fewer and larger cells with an increased DNA content. We propose that zebrafish Ubc9 is needed for G2/M transition and/or mitosis during vertebrate organogenesis, similar to what has been reported in *S. cerevisiae*.

MATERIALS AND METHODS

Cell Dissociation and Fluorescence-activated Cell Sorting Analysis

Embryos were anesthetized with tricaine (Westerfield, 2000) and decapitated. After transient storage in PBS/1 mM EDTA on ice, heads were incubated for 30 min in a 2 mg/ml papain solution in PBS/EDTA activated with L-cysteine (end concentration 30 ng/ml). Afterward, heads were transferred to fresh papain solution and triturated through a fire-polished glass pipette. This treatment was repeated three times in 15-min intervals, eventually leading to a single-cell suspension. Cells were harvested by centrifugation for 5 min at $1000 \times g$ and 4°C, resuspended in Ringer solution, counted, and adjusted to 5×10^6 cells/ml. Two hundred microliters of this cell suspension were fixed in 4 ml of ice-cold 70% ethanol and incubated over night on ice. Afterward, cells were harvested by centrifugation for 10 min at $1000 \times g$ and 4°C, taken up in propidium iodide (PI) buffer (980 μl PBS, 10 μl RNase [10 μg/ml], 10 μl PI [2 mg/ml]) at a cell density of 0.5×10^6 cells/ml, and analyzed on an LSRII flow cytometer (BD Biosciences, San Jose, CA). Data were evaluated using CellQuest software (BD Biosciences).

Generation of Constructs, mRNA Synthesis, and Microinjection

For expression constructs, the *ubc9.1* and *ubc9.2* coding regions were amplified via RT-PCR with primers containing EcoRI and XhoI restriction sites (Ubc9.1ECO 5′-CGG AAT TCA CCA TGT CTG GCA TTG CTC TGA GTC-3′; Ubc9.1XHO 5′-GGC GAG CTC ATC TCT CGG TGT CGC TTT ACG AC-3′; Ubc9.2ECO 5′-CGG AAT TCA CCA TGT CTG GTA TAG CAT TGA GTC-3′; Ubc9.2XHO 5′-CCG CTC GAG ATC TTG AGG TTT ACG GAC AGA AC-3′) with Pfu DNA polymerase (Stratagene, La Jolla, CA), and cloned into pCS2+ (Rupp *et al.*, 1994) or pSGH2 (Bajoghli *et al.*, 2004). The Ubc9.1 C93A mutation was introduced into the pCS2-*ubc9.1* using the QuikChange Site-Directed Mutagenesis Kit (Stratagene) and primers 5′-TCC GTC AGG AAC AGT GGC TCT TTC CAT CCT GGA G-3′ (sense), 5′-TCC TCC AGG ATG GAA AGA GCC ACT GTT CCT GAC GG-3′ (antisense). Capped RNA was prepared with the Message Machine kit (Ambion, Austin, TX). mRNA was diluted in 1× Danieu's buffer (Nasevicius and Ekker, 2000), and 1.5 nl was injected into 1–2-cell stage embryos (*HA-Sumo*: 25 pg per embryos; *ubc9.1* or *ubc9.1 C93A* mRNA: 75 pg per embryo).

Morpholino Injections

Antisense morpholino oligonucleotides (MOs, Gene Tools, Philomath, OR) were injected at the 1–2-cell stage, as previously described (0.5 pmol per embryo; 2 nl of 0.25 mM solution; Nasevicius and Ekker, 2000). The sequences of used MOs were as follows: *ubc9.1* MO 5′-TCG ACT CAG AGC AAT GCC AGA CA TG -3′, *ubc9.1* 5 mm control MO 5′-TgG ACT gAG AcC AAT GgC AcA CAT G-3′, *ubc9.2* MO 5′-GAC GAC TCA ATG CTA TAC CAG ACA T-3′.

Immunoblotting

For sumoylation assays, injected embryos were harvested at the 80% epiboly stage (8.5 hpf), and protein extracts were prepared as described (Westerfield, 2000). Proteins were separated via SDS-PAGE on 10% acrylamide/bis-acrylamide gels and blotted on Hybond P membranes (Amersham, GE Healthcare Europe, Munich, Germany). Immunoblotting was performed using an anti-HA (clone 12CA5; Roche Diagnostics, Mannheim, Germany), an anti-human Ubc9 (Cat. No. 610748; BD Biosciences Pharmingen, Heidelberg, Germany), or anti-pan cadherin antibody (No. C3678; Sigma, St. Louis, MO). To test the morpholino knockdown efficiency, MO-injected embryos were grown to the desired developmental stages, protein extracts were separated on 12% acrylamide/bis-acrylamide gels, and blots were probed with the anti-human Ubc9 antibody.

Tissue-labeling Procedures

Whole mount in situ hybridizations and immunohistochemistry were carried out as previously described (Hammerschmidt *et al.*, 1996). For riboprobe synthesis, plasmid *pSport1-ubc9.1* containing the full *ubc9.1* cDNA (1.3 kb) was linearized with SalI and transcribed with Sp6 RNA polymerase. The plasmid *pCRII-ubc9.2* containing a 0.8-kb fragment of the *ubc9.2* cDNA was linearized with HindIII and transcribed with T7 RNA polymerase. Riboprobes of *dlx2* and *dlx3* (Ellies *et al.*, 1997), *fgf3* (David *et al.*, 2002), *pax9a* (Nornes *et al.*, 1996), and *col2a1* and *sox9a* (Chiang *et al.*, 2001) were generated as previously described. For the in situ hybridizations shown in Figure 6, E and F, Fast Red (Roche Diagnostics) was used as substrate, yielding a fluorescent signal.

For protein detection the following primary antibodies were used: anti-p63 (4A4; mouse monoclonal; Santa Cruz Biotechnology, Santa Cruz, CA), antiphosphorylated histone H3 (pH3; rabbit polyclonal; Upstate Biotechnology, Charlottesville, VA), anti-Zn5 (mouse monoclonal; Zebrafish International Resource Center, University of Oregon, Eugene, OR), anti-GFP (goat polyclonal, Rockland Immunochemicals, Gilbertville, PA). For enzymatic detection (see Figure 5), biotinylated secondary antibodies and the Vectastain ABC kit (Axxora, Gruenberg, Germany) were used, as previously described (Hammerschmidt *et al.*, 1996). For fluorescent detection (see Figure 6), the following secondary antibodies were used: AlexaFluor 488–conjugated chicken anti-goat IgG, AlexaFluor 555–conjugated donkey anti-rabbit IgG, AlexaFluor 647–conjugated chicken anti-mouse IgG (Molecular Probes, Invitrogen, Karlsruhe, Germany).

5-Bromo-2′-deoxyuridine (BrdU) incorporation assays were performed essentially as described (Plaster *et al.*, 2006). After labeling, embryos were grown for 2 h at 28.5°C and fixed. Incorporated BrdU was detected using an anti-BrdU primary antibody (mouse monoclonal; Cat. No. 1170376; Roche Diagnostics) and a secondary AlexaFluor 647–conjugated goat anti-mouse IgG antibody (Molecular Probes).

For detection of apoptotic cells, TUNEL and acridine orange stainings were performed as previously described (Nowak *et al.*, 2005).

Confocal fluorescent images of immunostainings were taken on a LMS 510 Meta laser scanning microscope (Carl Zeiss, Jena, Germany), fluorescent images of acridine orange stainings on an Axiophot microscope (Carl Zeiss), using an ORCA ER C4742-95 digital camera (Hamamatsu, Bridgewater, NJ). Bright-field and fluorescent images were superimposed with Openlab software (Improvision, Lexington, MA).

Histology

Embryos were embedded in paraffin wax, and 6-μm-thick sections were cut with Feather S35 microtome blades on a Leica RM 2155 Microtome (Deerfield, MA). Sections were de-waxed using Rotihistol (Roth, Karlsruhe, Germany) and mounted in Roti-histokit (Roth).

Transplantations and Single-Cell Injections

For cell transplantations, donor embryos were injected with biotinylated dextran as lineage tracer (0.4%) and mRNA encoding constitutively active Nodal receptor Taram A, which targets cells to the endoderm (David and Rosa, 2001). At the sphere stage (4 hpf), 10–20 cells were transplanted from animal regions of donor to animal regions of recipient embryos. For single-cell injections, medial cells of 16–32-cell stage embryos were pressure-injected with biotinylated dextran and the *ubc9.1* full-match or 5 mis-match MO. Chimeric or injected embryos were grown to the desired developmental stages, fixed in 4% PFA, and stained with Alcian Blue, followed by visualization of transplanted or injected cells with the Vectastain ABC kit (Axxora).

RT-PCR

Zebrafish embryos were collected at specific time points after fertilization. Total RNA from whole embryos was isolated using Trizol-LS reagent (Invitrogen), and cDNA was generated using Superscript II reverse transcriptase (Invitrogen). For detection of *ubc9.1* and *ubc9.2* cDNAs, the same primers were used as for the cloning of the coding regions (see above). Sequences of *ef1α* control primers were: 5′-TCA CCC TGG GAG TGA AAC AGC-3′ (sense); 5′-ACT TGC AGG CGA TGT CAG CAG-3′ (antisense).

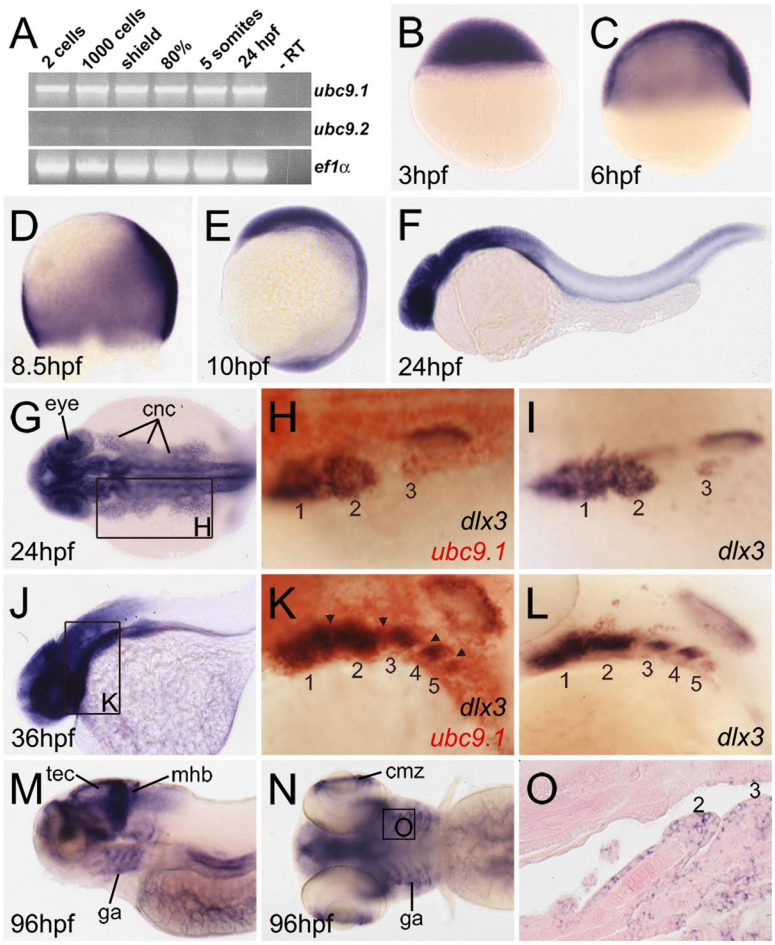

Figure 1. *ubc9.1* displays ubiquitous expression during gastrula stages, whereas larval expression is restricted to specific tissues. (A) Semiquantitative RT-PCR analysis of zebrafish *ubc9.1* and *ubc9.2* expression during embryonic development. As control, transcripts of the *ef1α* housekeeping gene were amplified. *ubc9.1* transcripts can be detected during all investigated stages, indicating maternal deposition of mRNA and zygotic expression of the gene. *ubc9.2* transcript can be detected at low levels during pregastrula stages, but not at later stages of development, suggesting that *ubc9.2* mRNA is maternally provided, whereas zygotic expression is absent. (B–O) In situ hybridization with *ubc9.1* antisense riboprobe at different stages of development. (B) 1000-cell stage (3 hpf); (C) 60% epiboly (6 hpf); (D) 80% epiboly (8.5 hpf); and (E) tailbud stage (10 hpf); at all stages the animal/anterior side of the embryos is to the top, and the dorsal side to the right; (F–I) 24 hpf. (F) Lateral view over entire embryo; *ubc9.1* shows prominent expression in the head region, including brain, eyes, and neural crest cells. (G) Dorsal view on head; region shown in (H and I) is boxed. (H) Magnified view on the developing pharyngeal arch area stained for *ubc9.1* mRNA (red) and *dlx3* mRNA (blue), a marker for cranial neural crest cells; in I, the red color has been washed out to show *dlx3* expression only; the *dlx3*-positive crest streams are numbered. (J–L) 36 hpf. (J) Lateral view over anterior half of embryo; *ubc9.1* expression is restricted to head region; region shown in K and L is boxed. (K and L) Magnified view on pharyngeal arch area stained for *ubc9.1* mRNA (red) and *dlx3* mRNA (blue; K), and after red color has been washed out (L); the *dlx3*-positive crest streams are numbered; *ubc9.1* is coexpressed with *dlx3* in cranial neural crest cells and without *dlx3* in endodermal pharyngeal pouches (indicated by arrow heads), and in mesenchymal cells posterior of the forming arches. (M–O) 96 hpf. (M) Lateral view of the head; (N) dorsal view of the head; *ubc9*.1 is expressed in late proliferative zones of the brain, such as in the tectum and the midhindbrain boundary region, in the ciliary marginal zone of the eye, and the pharyngeal pouches; region shown in O is boxed; (O) horizontal section through gill arches 2 and 3 (corresponding to pharyngeal arches 4 and 5); *ubc9.1* is expressed in the endoderm-derived pharyngeal pouches, whereas expression in differentiated chondrocytes has ceased. Abbreviations: cmz, ciliary marginal zone; cnc, cranical neural crest; eye, presumptive retinal cells of eye vesicles; ga, gill arches (pharyngeal arches 3–7); mhb, midhindbrain boundary; tec; tectum.

RESULTS

Zebrafish ubc9 Is Ubiquitously Expressed during Early Zebrafish Development and Becomes Restricted to Proliferative Zones at Later Stages

Two zebrafish *ubc9* genes have recently been identified, *ubc9.1* and *ubc9.2*, encoding very similar proteins of 158 amino acids that differ only by two amino acid residues. Compared with their mammalian counterparts, zebrafish Ubc9.1 is changed at two amino acid residues, whereas Ubc9.2 is changed at one position, only (Kurtzman and Schechter, 2001). As a first step to explore the role of Ubc9 during zebrafish development, we analyzed the spatial and temporal expression patterns of the two *ubc9* genes.

ubc9.2 was not detectable by in situ hybridization between 1000 cell stage (2 hours post fertilization; hpf) and 96 hpf, whereas weak signals were transiently detected during earliest stages of development via RT-PCR (Figure 1A; and not shown). This suggests that *ubc9.2* mRNA is maternally provided, but not zygotically expressed. *ubc9.1* mRNA is also maternally provided and, in contrast to *ubc9.2*, has a strong zygotic expression (Figure 1A). Whole mount in situ hybridization revealed ubiquitous *ubc9.1* expression during blastula and early gastrula stages, with slightly reduced expression levels in the ventral ectoderm (Figure 1, B–E; Bakkers *et al.*, 2005). At 24 hpf *ubc9.1* remains strongly expressed in brain, eyes, and spinal chord, whereas expression is absent from notochord and somites (Figure 1F). Prominent *ubc9.1* expression is also found in cranial neural crest cells that give rise to cartilaginous elements of the pharyngeal arches. Double stainings with the crest marker *dlx3* reveal that in addition *ubc9.1* is expressed in adjacent noncrest derived cells, representing either pharyngeal endoderm or mesenchyme tissue (Figure 1, G–L). During further development, expression in the CNS becomes confined to the ventricular zones of the brain and the ciliary marginal zones of the eyes, both of which are known as late proliferative zones (Figure 1, M and N). Expression in cranial crest cells ceases as they undergo terminal chondrocyte differentiation, morphologically visible by their "stack-of-coins"-like organization (Schilling and Kimmel, 1997). In contrast, expression in the pharyngeal endoderm persists (Figure 1O).

Loss of Maternal and Zygotic Ubc9 Function Leads to Embryonic Cell Death

To study the in vivo relevance of the zebrafish *ubc9* gene function, we performed gain- and loss-of-function studies. Over expression of either *ubc9.1* or *ubc9.2* by mRNA injection into one-cell stage embryos had no obvious effects on

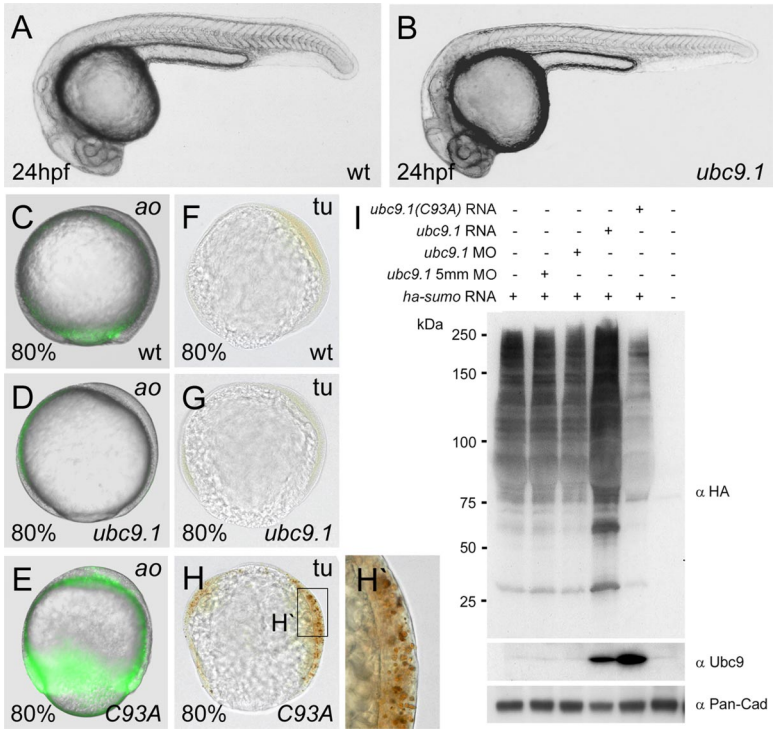

Figure 2. Loss of early Ubc9 function causes embryonic cell death. (A–H) Lateral overview of embryos at 24 hpf (A and B) and 80% epiboly (C–H). Embryos in C–E and F–H were stained with acridine orange (ao) and TUNEL (tu), respectively, to visualize apoptotic cells. (A and B) Embryo injected with wild-type *ubc9.1* mRNA (B) shows wild-type morphology as in uninjected sibling (A). (C–H) Embryos injected with mutant *ubc9.1* mRNA (C93A) encoding a dominant negative version of Ubc9 display widespread apoptosis (E, H, and H′; n = 52/58), whereas embryos injected with wild-type *ubc9.1*mRNA only have few apoptotic cells (D and G; n = 40/40), indistinguishable from the situation in uninjected siblings (C and F). (H′) Magnified view of region boxed in H. (I) Western blot of protein extracts from embryos injected either with an mRNA encoding HA-tagged Sumo1 alone, or HA-sumo1 RNA together with *ubc9.1* 5 mm MO, *ubc9.1* MO, or RNA encoding wild-type or dominant negative (*C93A*) Ubc9.1, probed with anti-HA, anti-Ubc9, and, as loading control, anti-pan-Cadherin antibody. Wild-type Ubc9.1 increases, whereas dominant negative Ubc9.1 reduces overall protein sumoylation levels. *ubc9.1* morphants display normal sumoylation levels, in line with the notion that at midgastrula stages, sumoylation is regulated by maternally provided Ubc9 protein (see also Figure 3).

embryonic development (Figure 2, A and B; and data not shown). To test whether despite this lack of developmental alterations, the increased dose of Ubc9 led to increased protein sumoylation levels, we injected the respective *ubc9* mRNA together with mRNA encoding an HA-tagged Sumo1, followed by the preparation of protein extracts from injected embryos, and immunoblotting with an anti-HA antibody. Indeed, compared with siblings injected with HA-Sumo, only, proteins of *ubc9* mRNA-injected embryos displayed strongly increased incorporation of HA-SUMO (Figure 2I), suggesting that hyper-sumoylation of proteins does not interfere with early zebrafish development.

To block Ubc9 function, we next injected mRNA encoding a dominant negative version of Ubc9 (dnUbc9; C93A). This protein is mutated in its Sumo-acceptor site, diminishing its E2 activity, while leaving its substrate binding capacity unaltered (Azuma *et al.*, 2003). Thereby over expressed protein competes with both maternally supplied and zygotically produced endogenous Ubc9 protein for substrate proteins. Consistently, injection of mRNA encoding dnUbc9 led a reduction of overall sumoylation activity in the immunoblotting experiments (Figure 2I). Morphologically, injected embryos displayed variable, but strong developmental defects during the first 24 h of development (data not shown). Because loss of Ubc9 function has previously been described to cause cell death during early mouse development, we stained injected zebrafish embryos at gastrula stages for apoptotic cells with acridine orange and using TUNEL. Although only few acridine orange or TUNEL-positive cells could be seen in uninjected siblings (Figure 2, C and F) or embryos injected with wild-type *ubc9.1* mRNA (Figure 2, D and G), embryos injected with *dn ubc9.1* mRNA displayed high numbers of apoptotic cells throughout all tissues (Figure 2, E, H, and H′). Together these data indicate that reduction of Ubc9 function during early stages of zebrafish development leads to widespread cell death, consistent with recent results obtained for Ubc9-deficient mice.

Loss of Zygotic Ubc9.1 Function Leads to Later Developmental Defects

To dissect the role of maternally supplied Ubc9 protein from that encoded by maternally and zygotically supplied *ubc9* mRNAs, we next blocked translation of *ubc9.1* and/or *ubc9.2* mRNAs by injecting specific antisense morpholino oligonucleotides into one-cell stage embryos. Of the two *ubc9* paralogues, only *ubc9.1* shows strong expression during embryonic and early larval development (see above; Figure 1A). Consistently, embryos injected with *ubc9.2* MO appeared normal during all investigated stages (24–120 hpf), whereas *ubc9.1* morphants started to display specific defects during the second day of development. At 48 hpf, *ubc9.1* morphants showed a reduction in the size of brain and eyes, and subtle malformations in craniofacial structures, whereas embryos injected with a 5 mis-match control morpholino (5-mm MO) showed no such phenotypes (Figure 3, A and B). This phenotype was not enhanced by coinjection of *ubc9.1* and *ubc9.2* MOs (data not shown), consistent with our finding that *ubc9.2* is not expressed during the corresponding stages of zebrafish development.

To demonstrate the specificity of the *ubc9.1* MOs, we performed rescue experiments. To this end we cloned the *ubc9.2* cDNA, which is not targeted by the *ubc9.1* MO, into pSGH2 vector (Bajoghli *et al.*, 2004). pSGH2 contains heat shock promoter elements that bidirectionally drive expression of eGFP and the inserted cDNA. In addition, the vector contains SceI meganuclease recognition sites for more efficient genomic integration. Empty pSGH2 (Figure 3E) or pSGH2-*ubc9.2* (Figure 3D) was coinjected with *ubc9.1* MO and SceI meganuclease at the one cell stage, and injected embryos were heat shocked at 8, 24, and 36 hpf. At 48 hpf, ~60% of the pSGH2-*ubc9.2* injected *ubc9.1* morphants displayed wild-type morphology, with a normal size of eyes and brain (compare Figure 3D with Figure 3C). Strikingly, all of these rescued embryos contained high numbers of

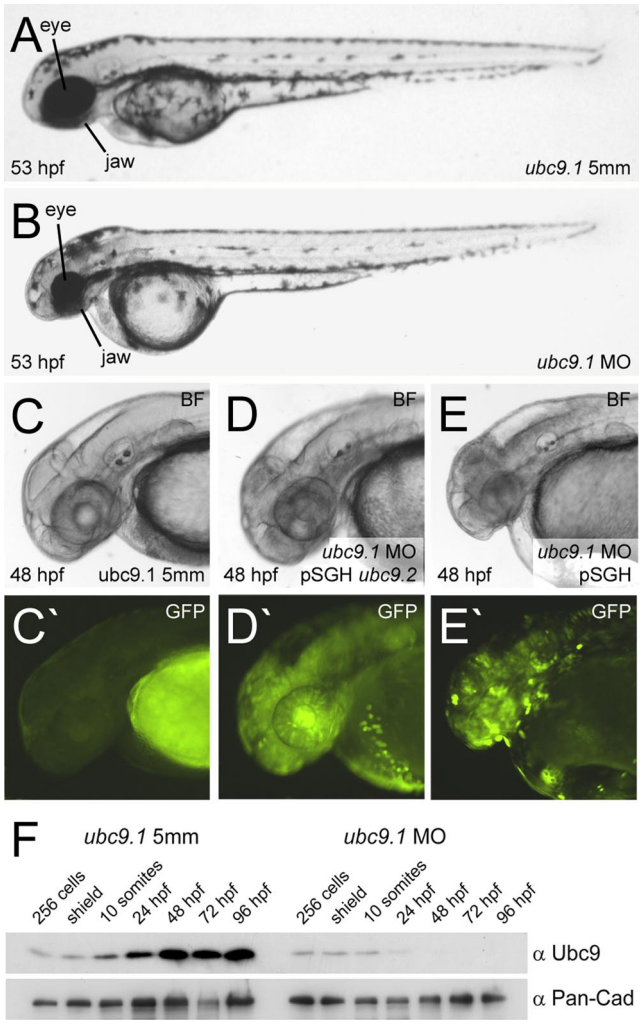

Figure 3. Loss of zygotic Ubc9.1 function causes defects in brain, eyes, and jaw. (A and B) Lateral overview of live embryos at 53 hpf. (A) *ubc9.1* 5 mm MO injected embryo; (B) *ubc9.1* MO injected embryo. *ubc9.1* morphants display a reduction in the size of brain and eyes and malformations in the jaw, whereas the overall body shape is normal. (C–E) Magnified lateral views of heads at 48 hpf. (C) *ubc9.1* 5 mm MO injected embryo; (D) embryo coinjected with *ubc9.1* MO and pSGH *ubc9.2* DNA, with a bicistronic heat-shock promoter driving expression of *egfp* and *ubc9.2*; (E) embryo injected with *ubc9.1* MO plus empty pSGH plasmid, driving *egfp* expression only. (C′–E′) shows GFP expression, marking transgene activation. *ubc9.2* overexpression rescues the *ubc9.1* MO induced phenotype (D and D′; n = 31/52), whereas overexpression of eGFP alone does not (E and E′; 0/35). Mean diameters of eye vesicles were as follows: (C) 0.25 mm ± 0.009; n = 5; (D) 0.24 mm ± 0.009; n = 5; (E) 0.19 mm ± 0.008; n = 5. Eye sizes of wild-type control embryos (C) and *ubc9.1* morphants after *ubc9.2* overexpression (D) are not significantly different (p = 0.03), indicating an efficient rescue of the morphant phenotype. In contrast, differences between wild-type control embryos (C) and *ubc9.1* morphants injected with empty vector (E) are significant ($p = 6.6E^{-5}$; calculated with Student's *t* test). (F) Western blot of embryonic protein extracts. Embryos were injected with either *ubc9.1* 5 mm MO (left) or *ubc9.1* MO (right) and harvested at the indicated developmental stages. The blot was probed with an anti-Ubc9 antibody or an anti-pan Cadherin antibody as a loading control. The *ubc9.1* MO used in this figure and Figures 4–8 efficiently blocks translation of endogenous *ubc9.1* mRNA, whereas the 5 mm MO does not. Note that in contrast to later stages, *ubc9.1* morphants up to 24 hpf display a Ubc9 band, which most likely represents residual maternally supplied Ubc9 protein.

GFP-positive cells in the head region, indicating efficient transgene activation, whereas most of the embryos with persistent morphant morphology (reduced eyes and brain) lacked GFP expression. In contrast, all embryos injected with empty pSGH2 and *ubc9.1* MO showed morphant morphology of unaltered strength, even when the head region contained many GFP-positive cells (Figure 3E). These data indicate that the morphant phenotype is specifically caused by a loss of Ubc9 function.

The late onset of the *ubc9.1* morphant phenotype in comparison to the phenotype observed upon over expression of the dominant negative Ubc9 points to the presence of maternal Ubc9 protein, which appears to compensate for the loss of zygotically generated Ubc9 protein during early developmental stages. To test this notion and to investigate the efficiency of the used *ubc9.1* MO, we performed anti-Ubc9 immunoblotting of protein extracts generated from *ubc9.1* morphant and control zebrafish at different stages of embryonic and larval development (Figure 3F). Before the onset of zygotic gene expression (256 cells stage) and during gastrulation stages (shield stage), *ubc9.1* 5 mm MO and *ubc9.1* MO injected embryos showed similar levels of Ubc9 protein. Because MOs targeting the start codon block translation of both maternally and zygotically supplied mRNA, these data indicate that the vast majority of Ubc9 protein present at these early stages is of maternal origin, whereas the contribution of de novo synthesized protein from maternally or zygotically supplied *ubc9.1* mRNA is minor. Consistently, overall protein sumoylation in *ubc9.1* morphants was indistinguishable from that of control embryos at gastrula stages (Figure 2I). However, from midsegmentation stages onward, Ubc9 protein levels in control embryos progressively rose, until a plateau was reached at 48 hpf, whereas in *ubc9*.1 MO morphants, Ubc9 protein levels started to decline, and no signal could be detected at 48 hpf or later. These results indicate that the used *ubc9.1* MO efficiently blocks translation of *ubc9.1* mRNA and that morphant larvae are devoid of Ubc9 protein between 48 and 96 hpf, whereas at earlier stages, maternally supplied Ubc9 protein is present. A similar high protein stability has recently been described for other maternally supplied housekeeping proteins, which could be detected throughout the first 2 d of development, compensating for the loss of zygotic gene products (Ryu *et al.*, 2005; Plaster *et al.*, 2006).

Loss of Ubc9.1 Affects Cartilaginous Elements of the Craniofacial System

To further characterize the Ubc9.1 loss-of-function phenotype, we analyzed the craniofacial defects in more detail. Alcian blue stainings of chondrocytes at 120 hpf revealed that the three first gill arches (pharyngeal arches 3–5) were strongly reduced in *ubc9.1* morphant larvae, whereas the more posterior arches were completely absent (pharyngeal arches 6–7). Also, the ceratohyal cartilage (dorsal component of the hyoid, pharyngeal arch 2) was affected and failed to point anteriorly, whereas the first pharyngeal arch (mandibulare) and other head cartilage elements were of rather normal shape (Figure 4, A and B). This progressive worsening of the phenotype from anterior to posterior arches reflects the time course of cartilage differentiation, which progresses in an anterior-to-posterior wave (Schilling and Kimmel, 1997), suggesting that posterior elements might be more strongly affected because of the progressive loss of maternal Ubc9 protein (see above and *Discussion*). Examination at higher magnifications showed that both in reduced and in normal cartilaginous elements, cells displayed abnormal morphology. In wild-type embryos and embryos in-

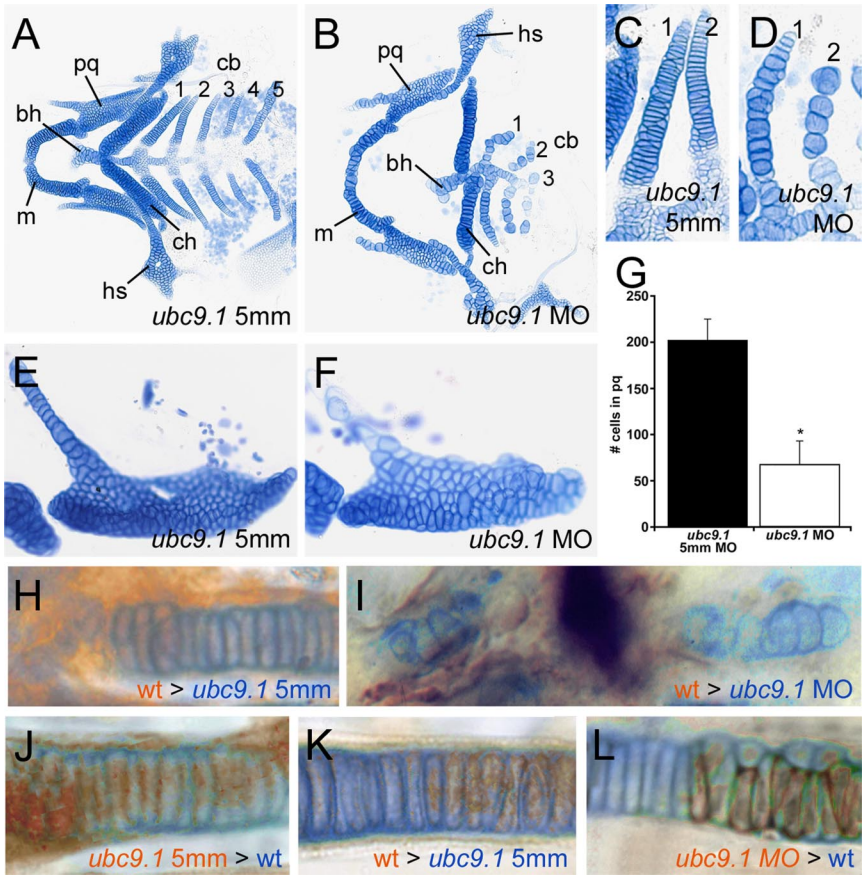

Figure 4. Loss of zygotic Ubc9.1 function causes a reduction of chondrocytes in craniofacial cartilaginous elements. (A–F) Preparations of cranial cartilaginous elements of larvae at 120 hpf, stained with alcian blue to visualize chondrocytes. (A, C, and E) *ubc9.1* 5 mm MO injected control larvae; (B, D, and F) *ubc9.1* MO injected larvae; anterior to the left. (A and B) Overview of flat mounts of all seven pharyngeal arches. In *ubc9.1* morphant larva (B) most jaw elements of the first and second pharyngeal arches (mandibulare and hyoid) are present and of relatively normal sizes and shapes. In contrast, the ceratobranchials of pharyngeal arches 3–7 (gill arches 1–5) are strongly reduced or absent. (C and D) Magnified view of gill arches 1 and 2. Chondrocytes of *ubc9.1* morphants (D) are of larger size and round, whereas in wild-type larvae (C), they show a "stack-of-coins"-like organization. (E and F) Magnified view of palatoquadrate of first jaw arch (mandibulare), which in *ubc9.1* morphant (F) is of rather normal shape and size, but consists of fewer and larger cells. (G) Quantification of total cell numbers in the palatoquadrate of control and *ubc9.1* morphant larvae. In morphants, palatoquadrate cells are reduced to approximately one-third of the number in control larvae ($p = 2e^{-19}$ as calculated with Student's *t* test; number of evaluated palatoquadrates: *ubc9.1* MO n = 20, *ubc9.1* 5 mm MO n = 19). (H–L) Magnified view on alcian blue–stained chimeric first gill arches with donor-derived cells in brown, anterior to the top. (H) Chimeric *ubc9.1* 5 mm MO injected embryo with pouch cells derived from an untreated control embryo; cartilage morphology is normal; (I) chimeric *ubc9.1* MO injected embryo with wild-type pouch cells on the left half-side; the cartilage phenotype on the left side is as strong as an the right side; (J) chimeric control embryo with pouch and cartilage cells derived from an *ubc9.1* 5 mm injected embryo; cartilage morphology is unchanged; (K) chimeric *ubc9.1* 5 mm injected embryo with cartilage cells derived from an untreated control embryo; cartilage morphology is unchanged; (L) chimeric control embryo with cartilage cells derived from an *ubc9.1* morphant; the morphology of *ubc9.1* morphant chondrocytes is altered compared wild-type chondrocytes, suggesting that Ubc9.1 has a cell-autonomous function within chondrocytes themselves. However, the phenotype is less severe than in nonchimeric morphants (compare with Figure 4D). bh, basihyal of second pharyngeal arch; ch, ceratohyal of second pharyngeal arch; cb, ceratobranchials of gill arches 1–5; hs, hyosymplectic of second pharyngeal arch; m, Meckel's cartilage of first pharyngeal arch; pq, palatoquadrate of first pharyngeal arch.

jected with the 5 mm MO, cells of the gill arches had a very ordered organization, appearing like a stack of coins, whereas in *ubc9.1* morphants, chondrocytes were significantly larger and of round shape (Figure 4, C and D). The same was true for cartilaginous elements of rather normal size and shape, e.g., the palatoquadrate, the dorsal element of the first arch (Figure 4, E and F). The number of chondrocytes in the palatoquadrate of *ubc9.1* morphants was reduced to approximately one-third of the number in wild-type siblings (Figure 4G), whereas remaining cells were enlarged, accounting for a rather normal size and shape of the element (Figure 4, E and F).

Ubc9.1 Is Required Both in Chondrocytes Themselves and in Other Tissues To Allow Proper Cartilage Formation

The cartilaginous components of the pharyngeal arches are formed from cranial neural crest cells, which at 16 hpf start to migrate in distinct streams from a position dorsal of the neural tube into ventrolateral positions of the head (Schilling and Kimmel, 1994; Wada *et al.*, 2005). At their final locations, neural crest cells interact with cells of the pharyngeal ectoderm and endoderm that form the pouch-like structures, separating the different crest streams and surrounding the later arches, as well as with noncrest derived mesenchymal cells to finally form the seven distinct pharyngeal arches (Schilling and Kimmel, 1994; Miller *et al.*, 2000; Piotrowski and Nüsslein-Volhard, 2000). Defective arch formation can therefore be caused by defects in the cranial neural crest population before, during, or after their migration (Yan *et al.*, 2002; Knight *et al.*, 2003), as well as by defects in pharyngeal pouch endoderm, ectoderm, or mesenchyme, which supply trophic support to the developing chondrocytes (Miller *et al.*, 2000; Piotrowski and Nusslein-Volhard, 2000; David *et al.*, 2002).

As described earlier, up to day 3 of development, *ubc9.1* is expressed in all of the tissues involved in arch formation (Figure 1). To identify the tissues requiring Ubc9.1 activity, we generated chimeric larvae. To study whether Ubc9.1 might be exclusively required in the pharyngeal endoderm, we tried to rescue the *ubc9.1* morphant phenotype by transplanting wild-type endoderm into morphant embryos. For this purpose, wild-type donor embryos were injected with a constitutively active form of the TGFβ type I receptor Taram-A (TarA*). This molecule does not only induce endodermal fates in ectopic cells (Alexander and Stainier, 1999), but also targets these cells to endodermal positions

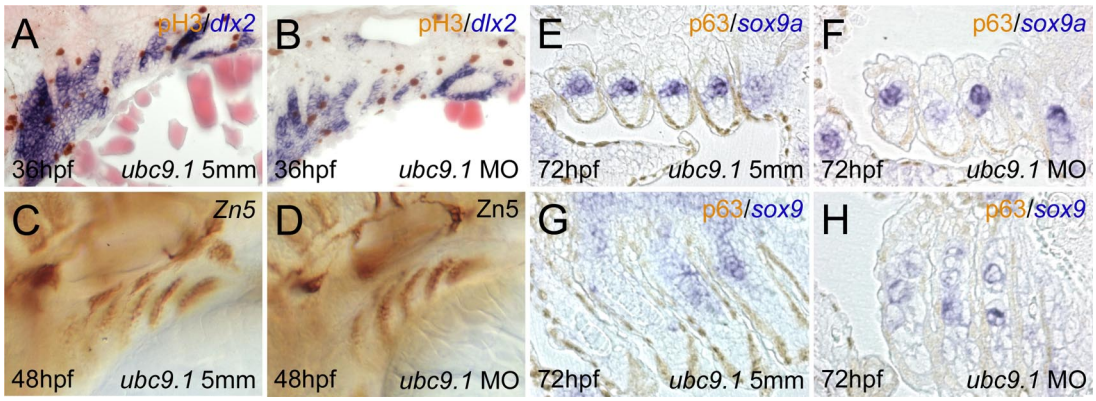

Figure 5. Ubc9.1 is dispensable for the specification and patterning of cranial neural crest and pharyngeal pouch cells. (A, C, E, and G) *ubc9.1* 5 mm MO injected embryos; (B, D, F, and H) *ubc9.1* MO injected embryos. (A and B) Saggital sections through forming pharyngeal arches, anterior to the left, dorsal to the top; embryos were stained for *dlx2* mRNA, a marker for cranial neural crest cells (blue) and phosphorylated Histone H3 (pH3) protein, a mitosis marker (brown). Morphant embryos display *dlx2* expression of normal pattern and intensity. (C and D) 48 hpf, lateral view on forming pharyngeal arches. Embryos are stained for Zn5, a marker for endodermal cells of the pharyngeal pouches; anterior to the left, dorsal to the top. Control and morphant are indistinguishable. (E–H) 72 hpf, horizontal sections at dorsal (E and F) and ventral position (G and H) through gill arches of left half-side, anterior to the left, medial to the top. Larvae were stained for *sox9a* mRNA (blue), a marker for differentiating chondrocytes (blue) and p63 protein (brown), marking the epidermal cells of the pouches. *sox9a* expression is unaffected in morphants (F and H), indicating that the crest cells follow their proper differentiation program. Cell numbers are already reduced and the remaining cells are bigger and unorganized as compared with control arches (E and G).

when transplanted into ectopic positions of wild-type hosts (homing effect; David and Rosa, 2001). Using this method to generate wild-type pouches in *ubc9.1* 5 mm MO injected embryos had no effect on cartilage morphology, indicating that Tar* overexpression does not interfere with the normal developmental program (Figure 4H). Chimeric *ubc9.1* morphant embryos with wild-type pharyngeal pouches generated in the same way showed the chondrocyte phenotype at unaltered strength (Figure 4I), ruling out that it is exclusively due to a requirement of Ubc9.1 in the pharyngeal endoderm. However, it is possible that Ubc9.1 is required in endodermal cells in addition to other cell types involved in arch formation.

To address whether the cartilage phenotype might be caused by a cell-autonomous effect of Ubc9.1 in chondrocytes themselves, we generated clones of *ubc9.1* morphant chondrocytes in wild-type animals by injection of *ubc9.1* MO together with a lineage tracer into a single central blastomere of a wild-type embryo at the 16-cell stage. Individual chondrocytes of obtained *ubc9.1* morphant clones, although surrounded by wild-type tissue, displayed altered shapes and did not intercalate properly (Figure 4L). Such morphological changes were never seen when *ubc9.1* 5-mm clones were generated in wild-type cartilage (Figure 4J) or vice versa (Figure 4K). This indicates that Ubc9.1 has a cell-autonomous function in chondrocytes. However, the chondrocyte phenotype in Ubc9.1-deficient clones was much weaker than in nonmosaic morphant larvae, suggesting that Ubc9.1 in addition affects chondrocyte development in a non-cell–autonomous manner.

ubc9.1 Is Dispensable for the Specification and Patterning of Pharygeal Arch and Pouch Tissues

As described in the *Introduction,* loss of Ubc9 function affects anterior-posterior patterning programs during *Drosophila* and *C. elegans* development. To study whether the observed differential defects in the cartilaginous elements of zebrafish *ubc9.1* morphants might result from similar patterning defects or from changes in the timing of cell specification processes, we investigated the expression of specification marker genes during different stages of arch formation. At 24 hpf, crest cells of the different streams become separated by a layer of ectoderm and endoderm. The first markers to reflect this pattern are *dlx2* in the cranial neural crest cells (Ellies *et al.,* 1997), *p63* in the ectoderm (Lee and Kimelman, 2002), and *fgf3* in the endoderm (David *et al.,* 2002). These initial patterns were indistinguishable between *ubc9.1* morphants and control embryos (Figure 5, A and B; and not shown). Between days 2–4 of development, crest cells differentiate to form chondrocytes, marked by the sequential expression of *sox9a* and *collagen 2a1* (Chiang *et al.,* 2001). Similarly, the pouch endoderm initiates Zn5 expression at day 2 (Piotrowski and Nüsslein-Volhard, 2000) and expression of *pax9a* (Nornes *et al.,* 1996) at day 3. Also, at these later stages, we could not detect any changes in the timing or expression levels of any of these marker genes in *ubc9.1* morphant embryos (Figure 5, C–F; and data not shown). However, consistent with results obtained via alcian blue stainings at 120 hpf (see above), the in situ hybridization with chondrocyte-specific markers did reveal aberrant cell morphology of chondrocytes, which was already apparent at 72 hpf. Chondrocytes were larger than in control embryos and showed no signs of intercalation (Figure 5, G and H). Together, these data suggest that Ubc9.1 function is dispensable for patterning processes or proper chondrocyte differentiation.

The Reduction of Chondrocyte Numbers in ubc9.1 Morphants Is Correlated with Reduced Cell Division Rates

To investigate whether the reduction in chondrocyte cell number in *ubc9.1* morphants is due to reduced proliferation or enhanced cell death of progenitor cells, we carried out antiphosphorylated histone H3 (pH3) immunostainings and BrdU incorporations studies, and TUNEL and acridine orange stainings, respectively. To be able determine ratios of cells in M-phase, pH3 stainings were performed in transgenic fish expressing membrane-bound GFP under the control of a cytoskeletal actin promoter, thereby visualizing cell boundaries (Cooper *et al.,* 2005). Furthermore, specimens

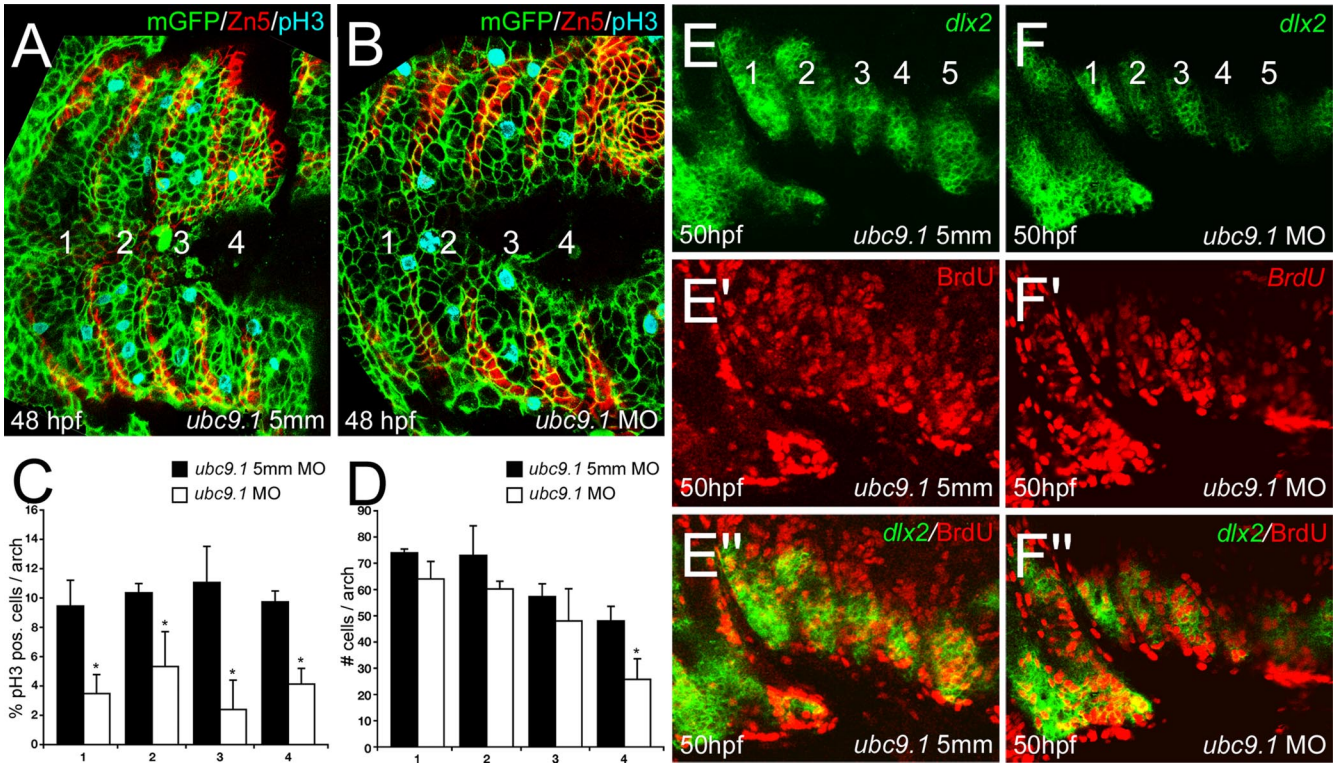

Figure 6. Loss of zygotic Ubc9.1 function causes a reduction of cranial chondrocyte precursors in mitosis. (A and B) Single confocal horizontal section through gill arches of *β-actin:mGFP* transgenic embryos (Cooper *et al.*, 2005) at 48 hpf, injected with (A) *ubc9.1* 5 mm MO or (B) *ubc9.1* MO; anterior to the left. Embryos were stained for GFP outlining individual cells (green), Zn5 (red, endodermal cells of pharyngeal pouches), and pH3 (cyan, cells in mitosis); the individual gill arches are numbered. The number of pH3-positive chondrocyte precursors is reduced in *ubc9.1* morphant (B). Note the cross-like mitotic figure in gill arch 2 in morphant, indicative for an 8n cell in anaphase. (C and D) Quantification of the results shown in A and B, taken from cell counts of consecutive sections through gill arches 1–4 (n = 3). ■, control embryos; □, *ubc9.1* morphants. (C) Percentage of pH3-positive chondrocyte precursors per arch; (D) total number of chondrocytes per arch. Although the total number of chondrocyte precursors in individual arches is still rather normal in morphant embryos, the percentage of pH3-positive cells is strongly reduced. Error bars, SD; asterisks, significant differences as calculated with Student's *t* test. (E and F) Single confocal horizontal section through gill arches of embryos at 50 hpf, injected with (E) *ubc9.1* 5 mm MO or (F) *ubc9.1* MO. Embryos were pulsed with BrdU to label S-phase cells at 48 hpf, fixed 2 h later and stained for *dlx2* mRNA (E and F), marking chondrocyte precursors and for incorporated BrdU (E′ and F′). (E″ and F″) Merged *dlx2* and BrdU images. There are no obvious differences in the percentages of BrdU-positive chondrocyte precursors in control and morphant embryos.

were stained for the endodermal pouch marker Zn5, allowing us to distinguish chondrocyte precursors of the different gill arches. Already at 48 hpf, *ubc9.1* morphants displayed a slight reduction in the number of chondrocyte precursors per arch, which was most prominent in the posterior gill arches (Figure 6, A, B, and D). Furthermore, the percentage of pH3-positive chondrocyte precursors was significantly reduced in all gill arches of *ubc9.1* morphants (Figure 6, A–C). Similarly reduced mitosis rates in precursor cells were found for more anterior cartilaginous elements, such as the palatoquadrate of the first pharyngeal arch (data not shown; see Figure 4, E and F, for reduced cell numbers), and for other late proliferative zones displaying *ubc9.1* expression, such as the ciliary marginal zones (CMZ) of the eyes. In accordance with the cartilaginous phenotype, the CMZs of *ubc9.1* morphants at 48 hpf consisted of fewer, but larger cells, with a significant reduction in the proportion of remaining cells expressing the mitotic marker pH3 (Supplementary Figure S1, C–F).

We also carried out BrdU incorporation studies to mark chondrocyte precursors in S-phase. However, in contrast to the measurements of cells in M-phase, no significant difference in the percentages of BrdU-positive chondrocyte or retinal precursor cells were found between *ubc9.1* morphants and control siblings at 48 hpf (Figure 6, E and F; and data not shown), suggesting that Ubc9.1 might specifically affect mitosis (see also below and *Discussion*).

Some, But Not All ubc9.1 Morphant Cells with Mitosis Defects Undergo Apoptosis

Employing TUNEL and acridine orange stainings, stronger apoptosis in chondrocytes of the gill arches of morphant larvae could first be detected at 96 hpf (Figure 7, E and F) ~48 h after the reduction in cell number had become apparent. Strikingly, apoptosis was most prominent in posterior gill arches, which were completely absent at 120 hpf (Figure 4B), whereas fewer or no acridine orange–positive cells at all were detected in the anterior-most pharyngeal arches (Figure 7, C and D). During earlier stages (24–72 hpf), cell death rates in gill arches of wild-type and morphant embryos were indistinguishable (Figure 7, A and B; and data not shown). In sum, these data indicate that the observed reduction in cell numbers in cartilaginous elements of the visceral head skeleton are largely due to reduced cell divisions, whereas apoptosis only accounts for the loss of the remaining chondrocyte precursors in the posterior-most gill arches. In contrast, in the eyes of *ubc9.1* morphant embryos, increased apoptosis was apparent from 24 hpf onward (data not

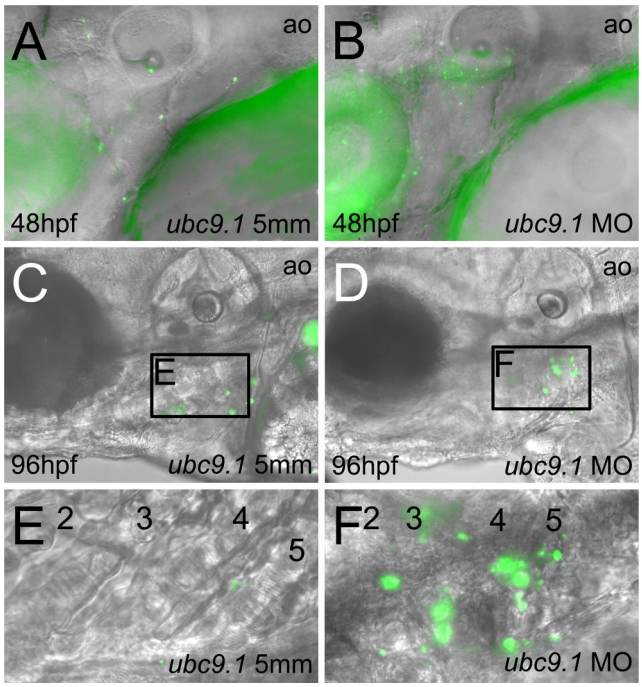

Figure 7. Apoptosis of chondrocyte precursors is restricted to posterior gill arches of *ubc9.1* morphants and occurs much later than the mitosis defects. (A–D) Lateral and (E and F) ventrolateral views on the forming arches of live zebrafish at (A and B) 48 hpf and (C–F) 96 hpf; anterior to the left. Embryos were injected with (A, C, and E) *ubc9.1* 5 mm MO or (B, D, and F) *ubc9.1* MO and stained with acridine orange (ao) to visualize apoptotic cells. In C and D, regions magnified and shown in a ventrolateral view in E and F are boxed. Individual gill arches in E and F are numbered. *ubc9.1* morphants display unaltered and low apoptosis rates in chondrocyte precursors at 48 hpf. At 96 hpf, strong apoptosis only occurs in gill arches 3–5, whereas more anterior arches show low cell death levels as in control larvae.

shown and Supplementary Figure S1, C and D), preceding the onset of defects during mitosis of retinal cells.

Loss of Ubc9.1 Function Causes an Accumulation of 4n and 8n Cells

In light of the different effects on pH3 expression and BrdU incorporation described above, we measured the DNA contents of cells from *ubc9.1* morphants and control embryos via PI stainings and fluorescence-activated cell sorting (FACS) analyses. Cells in G1 phase contain one copy of the diploid chromosome set (2n), whereas during S-phase, the total content of DNA increases gradually to the fully replicated value of 4n.

Comparing cell populations of heads from wild-type embryos at 36 and 48 hpf, we found a higher fraction of cells with a DNA content of 2n at 48 hpf. This accumulation of 2n cells reflects the higher percentage of differentiated postmitotic cells (G0-phase) in further developed embryos (Figure 8, A and E). Comparing wild-type with *ubc9.1* morphant heads, we could not detect any difference at 36 hpf (Figure 8, A and B). However at 48 hpf, *ubc9.1* morphant heads displayed a significant reduction in the proportion of cells with a DNA content of 2n (75 vs. 89%), whereas the proportion of cells with a higher DNA content was increased accordingly (for 4n: 14 vs. 6%; Figure 8, E and F). Notably, in morphant, but not wild-type heads, there was a small but reproducible population of cells with a DNA content of 8n (Figure 8, E

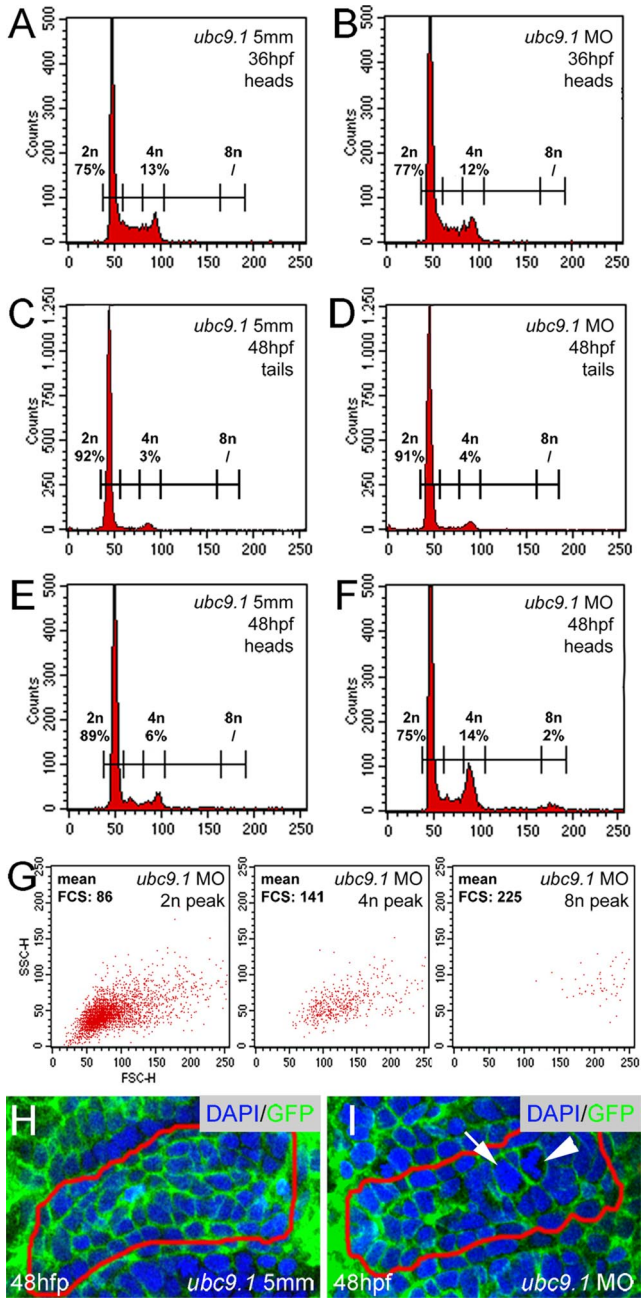

Figure 8. Loss of zygotic Ubc9.1 function causes an accumulation of cells with a DNA content of 4n or higher. (A–F) Representative histograms from FACS analysis of cell suspensions prepared from (A and B) 36 hpf heads, (C and D) 48 hpf tails, and (E and F) 48 hpf heads of embryos injected with (A, C, and E) *ubc9.1* 5 mm MO or (B, D, and F) *ubc9.1* MO, stained with PI. (A and B) At 36 hpf there is no obvious difference between control and *ubc9.1* morphant heads. The same is true for cells from tails at 48 hpf (C and D). However, cells from heads of 48 hpf *ubc9.1* morphants show an increased population of cells with a DNA content of 4n and a population of cells with a DNA content of 8n, which is absent in *ubc9.1* 5 mm MO-injected embryos (E and F). (G) Sideward scatter (SSC) and forward scatter (FSC) dot-plots of cells of the 2n, 4n, and 8n peak of *ubc9.1* MO head at 48 hpf, shown in F (gated populations are indicated with brackets). Mean FSC values reflect average cell sizes. (H and I) Confocal sagittal sections through gill arches of *β-actin:mGFP* transgenic embryos at 50 hpf, injected with (H) *ubc9.1* 5 mm MO or (I) *ubc9.1* MO; anterior to the top. Embryos were stained for GFP, marking cell boundaries and for DAPI, visualizing DNA in

and F), suggesting that 4n cells can go through another round of DNA replication. This is consistent with the cross-like mitotic figures seen in some of the chondrocyte precursors stained with the pH3 antibody (Figure 6B). Both the increase in the 4n cell population and the appearance of an 8n peak were specific to the head tissue. Cells prepared from morphologically unaffected tissue like the tail (see Figure 3, A and B), which at this time largely consists of postmitotic cells, showed an indistinguishable cell cycle profile between controls and morphants (Figure 8, C and D). This increase in DNA content of cells of *ubc9.1* morphant heads correlates with an increase in cell sizes. Thus, on sideward–forward scatter plots, cells of the 8n and 4n populations displayed 2.6 or 1.6-fold higher mean size values than the 2n population (Figure 8G). Likewise, in situ, larger chondrocytes in the branchial arches of *ubc9.1* morphants displayed larger DAPI-positive nuclei than normally sized chondrocytes of control embryos (Figure 8, H and I).

Together, this suggests that *ubc9.1* morphant cells display compromised entry or completion of M-phase, whereas further DNA replication or cell differentiation is unaffected. Thus, only some cells undergo apoptosis, whereas others become polyploid, grow to a larger size, and give rise to organs of roughly normal architecture.

DISCUSSION

Protein sumoylation affects multiple cellular processes, and the list of sumoylated proteins is continuously growing, raising the question about the primary impact of sumoylation on the entire organism. Thus far, ubc9 loss-of-function studies have been largely carried out in invertebrate systems (*S. cerevisiae*, *S. pombe*, *C. elegans*, and *D. melanogaster*). Only recently, *Ubc9*-deficient mice have been described. However, because of early lethality of mutants shortly after implantation, studies had to be carried out with cultured blastocystes (Nacerddine *et al.,* 2005). Here, we report *ubc9* loss-of-function studies in intact zebrafish embryos. In accordance with data obtained in mouse, we show that early Ubc9 function is necessary for cell survival during zebrafish gastrulation. Using antisense-mediated knock down of zygotic Ubc9, we in addition find that during organogenesis, Ubc9.1 is indispensable for mitosis. However, despite failed mitosis, *ubc9.1*-morphant cells can properly differentiate (progression to G1/GO phase) and, to some extent, can even reenter S-phase, creating a cell population with a DNA content higher than 4n.

Ubc9 Is Expressed in Proliferative Tissues

The zebrafish genome contains two *ubc9* genes. Both of them are expressed during oogenesis, and the respective mRNAs are deposited in the eggs. However, only one of them, *ubc9.1*, is zygotically expressed by the embryo itself. During gastrula stages, it displays a ubiquitous expression, with slightly reduced levels in the ventral ectoderm (compare with Bakkers *et al.,* 2005). During later development *ubc9.1* expression becomes more restricted, with highest transcript levels in the ciliary marginal zone of the eye, the ventricular zones of the brain, and the pharyngeal pouches. All of these domains are zones of late cell proliferation, as indicated by the expression of various marker genes, such as *pcna*, various *cyclins*, and *DNA polymerase delta1*, as well as by their high BrdU-incorporating activity (Plaster *et al.,* 2006). This *ubc9.1* expression pattern is in line with a role during cell proliferation in zebrafish larvae and with functional data obtained in other systems. Thus, Ubc9 has been implicated in various aspects of cell cycle control like chromosome condensation and segregation (Tanaka *et al.,* 1999; Azuma *et al.,* 2003) and the regulation of cyclin stability (Seufert *et al.,* 1995; Dieckhoff *et al.,* 2004), as well as in different DNA repair mechanisms (Hardeland *et al.,* 2002; Hoege *et al.,* 2002; Stelter and Ulrich, 2003).

Increased Protein Sumoylation Does Not Influence Early Zebrafish Development

To address the in vivo relevance of Ubc9 function during zebrafish development, we carried out both gain- and loss-of-function studies. For gain-of-function studies, *ubc9.1* mRNA was injected into one-cell stage embryos. Consistent with the reported function of Ubc9 as an E2 Sumo-conjugating enzyme, injected embryos displayed a significant increase in protein sumoylation, suggesting that the endogenous level of Ubc9 protein is the rate-limiting factor determining the degree of protein sumoylation. However, despite protein hyper-sumoylation, injected embryos showed unaltered morphology and normal apoptosis rates. This suggests that embryos can tolerate increased steady state levels of sumoylated proteins. Similar data were obtained in mouse, where loss of the desumoylating enzyme SENP1 leads to placental abnormalities, whereas fetal development itself is normal, despite overall increased Sumo conjugation (Yamaguchi *et al.,* 2005).

The Stability of Ubc9 Protein and the Kinetics of Phenotype Development in Antisense-treated Zebrafish Embryos

In contrast to the gain-of-function studies, striking defects during zebrafish development were obtained upon loss of Ubc9 function and protein hypo-sumoylation. Our analyses indicate that there are three different kinds of *Ubc9* gene products present during early stages of zebrafish development: maternally contributed Ubc9 protein, maternally supplied *ubc9* mRNA, and zygotic *ubc9.1* transcripts, which start to be made by the embryo after midblastula transition, ~3 h after fertilization (Kane and Kimmel, 1993). Two different approaches were taken to block Ubc9 function. To inactivate Ubc9 protein from all three sources, we injected mRNA encoding a dominant negative version of Ubc9. This treatment leads to a significant reduction, but not complete loss of protein sumoylation at late gastrula stages (10 hpf), therefore most likely creating a hypomorphic, rather than an amorphic situation. As a second approach, we injected antisense morpholino oligonucleotides, which specifically block the translation of maternally supplied and zygotic *ubc9* mRNAs, while not affecting maternally supplied Ubc9 protein. Our Western blot analyses show that under these conditions, considerable amounts of Ubc9 protein were still present until 24 hpf, whereas embryos were completely devoid of Ubc9 protein at 48 hpf and later developmental stages. This observation is consistent with data gathered from the phenotypic analysis of morphant embryos, which first develop defects around 48 hpf, indicating that maternal Ubc9 protein is sufficient to compensate for the loss of zygotic Ubc9 protein during earlier stages of development. The high stability of maternal Ubc9 protein is consistent with data obtained for other maternally supplied zebrafish proteins (Ryu *et al.,* 2005; Plaster *et al.,* 2006). In addition, it is consistent with data obtained for Ubc9 in a chick cell line

Figure 8 (cont). nuclei. The red line marks a single branchial arch. *ubc9.1* morphant arches contain enlarged cells with enlarged nuclei (arrow) or abnormal mitotic figures (arrowhead).

(Hayashi *et al.*, 2002), where Ubc9 protein was still detectable 2 d after gene inactivation, and sumoylated proteins could even be seen for 1 additional day (Hayashi *et al.*, 2002).

However, we want to point out that our Ubc9 Western blot analyses were done with extracts from whole embryos, although there might be differences among different tissues, consistent with the different kinetics of phenotype development. In *ubc9.1* morphant embryos, apoptosis in the eyes is already apparent at 24 hpf (Supplementary Figure S1; and unpublished observations), whereas apoptosis in cranial cartilage, if at all, is not observed before 96 hpf. These different response times of different cell types can have various reasons. They could result from differences in the stability of Ubc9 protein and/or sumoylated proteins in the different cell types, for instance, as a consequence of different proliferation rates. Strongly proliferating tissues should have a higher turnover of sumoylated proteins, because sumoylation can be subject to cell cycle control (Azuma *et al.*, 2003; Dieckhoff *et al.*, 2004). In addition, because proliferation is linked to tissue growth, the cellular concentration of maternal Ubc9 should drop faster in tissues with high proliferation rates. Along these lines, cartilage-forming neural crest population cells start to proliferate rather late in comparison to retinal cells of the eyes. Alternatively or in addition, different cell types may require different concentrations of Ubc9 protein. Along these lines, the progressively dropping levels of maternal Ubc9 protein would first affect cells that require highest Ubc9 levels (as in the eyes), whereas other cell types would only be affected much later (as in the cartilage), or not at all (as in tissues largely consisting of postmitotic cells).

Loss of Ubc9 Leads to Compromised Mitosis and Cellular Overgrowth

Knockout studies in mouse have revealed multiple roles of Ubc9 required for proper nuclear function in proliferating cells of the early embryo, such as regulation of overall nuclear organization, chromosome segregation, and nucleocytoplasmic transport (Kuehn, 2005; Nacerddine *et al.*, 2005). In comparison, chondrocyte precursors in *ubc9.1* morphants appear to have rather specific defects. They are reduced in number and grow to a larger cellular size, but differentiate normally (Figure 4). The primary reason for the reduced cell number most likely is compromised or blocked mitosis. At 48 hpf, when the number of chondrocyte precursors in *ubc9.1* morphants is still quite normal, they display a significant reduction in the proportion of cells positive for the M-phase marker pH3 (Figure 6). In contrast, the proportion of cells incorporating BrdU is normal. The same is true for the ciliary marginal zone of the retina, another investigated late proliferative tissue (Supplementary Figure S1). Consistently, our FACS analyses revealed a significant increase in the number of cells with a DNA content of 4n. Strikingly, we also observed a small population of cells with a DNA content of 8n, suggesting that failed mitosis does not prevent cells from undergoing a further round of DNA replication. This is consistent with the mitotic figures observed for some chondrocyte precursors of *ubc9.1* morphant embryos (Figures 6B and 8I). The shape of the mitotic figures further indicates that blockage in mitosis occurs during anaphase, when chromatids separate (compare with Figure 4G in Nacerddine *et al.*, 2005). Interestingly, in *Drosophila* embryos, Rca1, an inhibitor of the anaphase-promoting complex (APC), has been shown to be required for entry into mitosis. Loss of Rca1 leads to cells with larger nuclei and increased DNA content (Grosskortenhaus and Sprenger, 2002), as described here for *ubc9.1* morphants, making APC components or regulators good candidates for Ubc9 targets mediating its effect during mitosis control. Another good candidate is topoisomerase II, which in *Xenopus* egg extracts has been shown to be sumoylated, while treatment with dominant negative Ubc9 leads to persistent association of topoisomerase with mitotic chromosomes and to a blockage of sister chromatid separation at the metaphase-anaphase transition (Azuma *et al.*, 2003).

A similar continuation of DNA replication in the absence of mitotic divisions also occurs naturally in animal and plant cells that follow an endoreplication program (Edgar and Orr-Weaver, 2001). One example are the polytene salivary gland cells of *D. melanogaster*. Also in this case, cell size is correlated with ploidy, and salivary gland cells remain smaller when endoreplication is inhibited (Follette *et al.*, 1998; Weiss *et al.*, 1998). Here we show that *ubc9.1* morphant cells with a DNA content of 8n are larger in size than 2n and 4n cells (Figure 8, G–I), suggesting a similar direct correlation between cell size and ploidy. In addition, increased cell size might be due to alterations in external signals that dictate growth rates independently of cell cycle progression. It has previously been shown in cell culture systems that growth factor stimulation can lead to cell growth (volume increase), whereas cell cycle progression is blocked (Conlon *et al.*, 2001; Dolznig *et al.*, 2004). A scenario like this might explain the results obtained in our chimerae analyses, where *ubc9.1* morphant chondrocytes showed a less pronounced size phenotype when exposed to a wild-type environment.

Importantly, despite the blockage of mitosis, *ubc9.1* morphant chondrocyte precursors of the anterior pharyngeal arches were viable and underwent normal differentiation. Recently, it has been shown that the activity of Sox9, a key regulator of chondrocyte differentiation in all vertebrates, including zebrafish (Yan *et al.*, 2002), is regulated by sumoylation (Taylor and LaBonne, 2005). However, the net effect of such Sox9 sumoylation seems to be tissue-dependent. In the neural crest, from which chondrocytes derive, Sox9 sumoylation was found to be dispensable for its specification-promoting activity, consistent with our findings that chondrocyte differentiation is not compromised in *ubc9.1* morphants.

Together, our data suggest that in anterior chondrocytes, the primary function of Ubc9 is concerned with the regulation of mitosis and cellular growth, whereas other roles of Ubc9, such as the regulation of nuclear architecture, nucleocytoplasmic transport and the regulation of transcription factors are less essential. Alternatively, these other processes might require lower concentrations of Ubc9 protein, so that residual maternal protein is sufficient to take care of these functions (see also above). Also, it has to be pointed out that such anterior chondrocyte precursors blocked in mitosis would most likely have differentiated after one or two additional cell cycles. Thus, they were caught by loss of Ubc9 function in a rather advanced developmental state.

Ubc9 Is Required for Tissue-specific Cell Viability

In addition to the mitosis defects discussed above, *ubc9.1* morphant zebrafish display apoptosis in the eyes (Supplementary Figure S1) and the posterior pharyngeal arches (Figure 7). In the case of the eyes, apoptosis coincides with or even precedes detectable defects in mitosis, whereas in the posterior arches, it could only be detected 48 h after the mitosis defects. Also, we obtained widespread apoptosis when blocking Ubc9 function in early embryos via injection of mRNA encoding a dominant negative version of Ubc9 (Figure 2). The unlinked onsets of mitosis defects versus apoptosis in different cell types or regions of *ubc9.1* mor-

phants suggests that cell death occurs independently of compromised mitosis, a notion further supported by the viability of tetraploid zebrafish, which can be generated by blocking the second meiotic division shortly after egg fertilization (Streisinger *et al.*, 1981).

We can only speculate about the reasons for the apoptosis in *ubc9.1* morphant zebrafish. Sumoylation has previously been reported to negatively regulate Fas and TNF receptor 1–activated apoptosis (Okura *et al.*, 1996). During normal eye morphogenesis, a subset of retinal cells undergoes programmed cell death (Cole and Ross, 2001). In this light, the even higher death rate in ubc9.1 morphants might be due to a higher sensitivity of retinal cells to such endogenous death signals. In chondrocytes, apoptosis during normal development is less prominent (Cole and Ross, 2001), suggesting that the death of posterior arch chondrocytes seen in morphant larvae might have other reasons. Comparably late apoptosis is only observed much later than the defects during cell cycle progression, suggesting that here cell viability might dependent on another function of Ubc9. Comparably late apoptosis is also seen in Ubc9-deficient chick cell line where cell death coincides with the loss of sumoylated RanGAP1, a factor needed for nuclear import of proteins (Hayashi *et al.*, 2002). Similarly, in *Ubc9* knock out mice, mislocalization of RanGAP1 and loss of nuclear integrity were proposed to be likely reasons for the observed cell death (Nacerddine *et al.*, 2005). Thus, a similar scenario could underlie the late cell death observed in posterior chondrocytes of *ubc9.1* morphants. However, clearly, this only affects late differentiating cells, whereas cells of the same type that differentiate slightly earlier are viable, displaying mitosis defects only, thereby highlighting the pivotal role of Ubc9 during mitosis and chromatid separation.

ACKNOWLEDGMENTS

We thank Jacek Topczewski and Lilianna Solnica-Krezel for providing us with the *β-actin:mGFP* transgenic zebrafish line before publication and Frederic Rosa (*TarA**), Marc Ekker (*dlx2*, *dlx3*), and Thomas Czerny (*pSGH2*) for sending plasmids. In addition, we thank Conrad Bleul, Andreas Würch, and Petra Kindle for help with FACS sorting and confocal microscopy and Donatus Boensch for zebrafish animal care. Work in the laboratory of M.H. was supported by the Max-Planck Society and the National Institutes of Health Grant 1R01-GM63904. M.N. thanks the Boehringer Ingelheim Fonds, Heidesheim, for his long-term predoctoral fellowship and Michael Brand for support during the revisions of the manuscript.

REFERENCES

Alexander, J., and Stainier, D. Y. (1999). A molecular pathway leading to endoderm formation in zebrafish. Curr. Biol. *9*, 1147–1157.

al-Khodairy, F., Enoch, T., Hagan, I. M., and Carr, A. M. (1995). The *Schizosaccharomyces pombe* hus5 gene encodes a ubiquitin conjugating enzyme required for normal mitosis. J. Cell Sci. *108*(Pt 2), 475–486.

Azuma, Y., Arnaoutov, A., and Dasso, M. (2003). SUMO-2/3 regulates topoisomerase II in mitosis. J. Cell Biol. *163*, 477–487.

Bachant, J., Alcasabas, A., Blat, Y., Kleckner, N., and Elledge, S. J. (2002). The SUMO-1 isopeptidase Smt4 is linked to centromeric cohesion through SUMO-1 modification of DNA topoisomerase II. Mol. Cell *9*, 1169–1182.

Bajoghli, B., Aghaallaei, N., Heimbucher, T., and Czerny, T. (2004). An artificial promoter construct for heat-inducible misexpression during fish embryogenesis. Dev. Biol. *271*, 416–430.

Bakkers, J., Camacho-Carvajal, M., Nowak, M., Kramer, C., Danger, B., and Hammerschmidt, M. (2005). Destabilization of DeltaNp63alpha by Nedd4-mediated ubiquitination and Ubc9-mediated sumoylation, and its implication on dorsoventral patterning of the zebrafish embryo. Cell Cycle *4*, 790–800.

Chiang, E. F., Pai, C. I., Wyatt, M., Yan, Y. L., Postlethwait, J., and Chung, B. (2001). Two sox9 genes on duplicated zebrafish chromosomes: expression of similar transcription activators in distinct sites. Dev. Biol. *231*, 149–163.

Cole, L. K., and Ross, L. S. (2001). Apoptosis in the developing zebrafish embryo. Dev. Biol. *240*, 123–142.

Conlon, I. J., Dunn, G. A., Mudge, A. W., and Raff, M. C. (2001). Extracellular control of cell size. Nat. Cell Biol. *3*, 918–921.

Cooper, M. S., Szeto, D. P., Sommers-Herivel, G., Topczewski, J., Solnica-Krezel, L., Kang, H. C., Johnson, I., and Kimelman, D. (2005). Visualizing morphogenesis in transgenic zebrafish embryos using BODIPY TR methyl ester dye as a vital counterstain for GFP. Dev. Dyn. *232*, 359–368.

David, N. B., and Rosa, F. M. (2001). Cell autonomous commitment to an endodermal fate and behaviour by activation of Nodal signalling. Development *128*, 3937–3947.

David, N. B., Saint-Etienne, L., Tsang, M., Schilling, T. F., and Rosa, F. M. (2002). Requirement for endoderm and FGF3 in ventral head skeleton formation. Development *129*, 4457–4468.

Desterro, J. M., Thomson, J., and Hay, R. T. (1997). Ubc9 conjugates SUMO but not ubiquitin. FEBS Lett. *417*, 297–300.

Dieckhoff, P., Bolte, M., Sancak, Y., Braus, G. H., and Irniger, S. (2004). Smt3/SUMO and Ubc9 are required for efficient APC/C-mediated proteolysis in budding yeast. Mol. Microbiol. *51*, 1375–1387.

Dolznig, H., Grebien, F., Sauer, T., Beug, H., and Mullner, E. W. (2004). Evidence for a size-sensing mechanism in animal cells. Nat. Cell Biol. *6*, 899–905.

Edgar, B. A., and Orr-Weaver, T. L. (2001). Endoreplication cell cycles: more for less. Cell *105*, 297–306.

Ellies, D. L., Stock, D. W., Hatch, G., Giroux, G., Weiss, K. M., and Ekker, M. (1997). Relationship between the genomic organization and the overlapping embryonic expression patterns of the zebrafish dlx genes. Genomics *45*, 580–590.

Epps, J. L., and Tanda, S. (1998). The *Drosophila* semushi mutation blocks nuclear import of bicoid during embryogenesis. Curr. Biol. *8*, 1277–1280.

Follette, P. J., Duronio, R. J., and O'Farrell, P. H. (1998). Fluctuations in cyclin E levels are required for multiple rounds of endocycle S phase in *Drosophila*. Curr. Biol. *8*, 235–238.

Gill, G. (2003). Post-translational modification by the small ubiquitin-related modifier SUMO has big effects on transcription factor activity. Curr. Opin. Genet. Dev. *13*, 108–113.

Gong, L., Kamitani, T., Fujise, K., Caskey, L. S., and Yeh, E. T. (1997). Preferential interaction of sentrin with a ubiquitin-conjugating enzyme, Ubc9. J. Biol. Chem. *272*, 28198–28201.

Grosskortenhaus, R., and Sprenger, F. (2002). Rca1 inhibits APC-Cdh1(Fzr) and is required to prevent cyclin degradation in G2. Dev. Cell *2*, 29–40.

Hammerschmidt, M., Serbedzija, G. N., and McMahon, A. P. (1996). Genetic analysis of dorsoventral pattern formation in the zebrafish: requirement of a BMP-like ventralizing activity and its dorsal repressor. Genes Dev. *10*, 2452–2461.

Hardeland, U., Steinacher, R., Jiricny, J., and Schar, P. (2002). Modification of the human thymine-DNA glycosylase by ubiquitin-like proteins facilitates enzymatic turnover. EMBO J. *21*, 1456–1464.

Hari, K. L., Cook, K. R., and Karpen, G. H. (2001). The *Drosophila* Su(var)2–10 locus regulates chromosome structure and function and encodes a member of the PIAS protein family. Genes Dev. *15*, 1334–1348.

Hayashi, T., Seki, M., Maeda, D., Wang, W., Kawabe, Y., Seki, T., Saitoh, H., Fukagawa, T., Yagi, H., and Enomoto, T. (2002). Ubc9 is essential for viability of higher eukaryotic cells. Exp. Cell Res. *280*, 212–221.

Hoege, C., Pfander, B., Moldovan, G. L., Pyrowolakis, G., and Jentsch, S. (2002). RAD6-dependent DNA repair is linked to modification of PCNA by ubiquitin and SUMO. Nature *419*, 135–141.

Johnson, E. S., and Blobel, G. (1997). Ubc9p is the conjugating enzyme for the ubiquitin-like protein Smt3p. J. Biol. Chem. *272*, 26799–26802.

Johnson, E. S., and Gupta, A. A. (2001). An E3-like factor that promotes SUMO conjugation to the yeast septins. Cell *106*, 735–744.

Jones, D., Crowe, E., Stevens, T. A., and Candido, E. P. (2002). Functional and phylogenetic analysis of the ubiquitylation system in *Caenorhabditis elegans*: ubiquitin-conjugating enzymes, ubiquitin-activating enzymes, and ubiquitin-like proteins. Genome Biol. *3*, RESEARCH0002.

Kagey, M. H., Melhuish, T. A., and Wotton, D. (2003). The polycomb protein Pc2 is a SUMO E3. Cell *113*, 127–137.

Kane, D. A., and Kimmel, C. B. (1993). The zebrafish midblastula transition. Development *119*, 447–456.

Knight, R. D., Nair, S., Nelson, S. S., Afshar, A., Javidan, Y., Geisler, R., Rauch, G. J., and Schilling, T. F. (2003). lockjaw encodes a zebrafish tfap2a required for early neural crest development. Development *130*, 5755–5768.

Kuehn, M. R. (2005). Mouse Ubc9 knockout: many path(way)s to ruin. Dev. Cell *9*, 727–728.

Kurtzman, A. L., and Schechter, N. (2001). Ubc9 interacts with a nuclear localization signal and mediates nuclear localization of the paired-like homeobox protein Vsx-1 independent of SUMO-1 modification. Proc. Natl. Acad. Sci. USA *98*, 5602–5607.

Lee, H., and Kimelman, D. (2002). A dominant-negative form of p63 is required for epidermal proliferation in zebrafish. Dev. Cell *2*, 607–616.

Matunis, M. J., Coutavas, E., and Blobel, G. (1996). A novel ubiquitin-like modification modulates the partitioning of the Ran-GTPase-activating protein RanGAP1 between the cytosol and the nuclear pore complex. J. Cell Biol. *135*, 1457–1470.

Miller, C. T., Schilling, T. F., Lee, K., Parker, J., and Kimmel, C. B. (2000). Sucker encodes a zebrafish Endothelin-1 required for ventral pharyngeal arch development. Development *127*, 3815–3828.

Muller, S., Matunis, M. J., and Dejean, A. (1998). Conjugation with the ubiquitin-related modifier SUMO-1 regulates the partitioning of PML within the nucleus. EMBO J. *17*, 61–70.

Nacerddine, K., Lehembre, F., Bhaumik, M., Artus, J., Cohen-Tannoudji, M., Babinet, C., Pandolfi, P. P., and Dejean, A. (2005). The SUMO pathway is essential for nuclear integrity and chromosome segregation in mice. Dev. Cell *9*, 769–779.

Nasevicius, A., and Ekker, S. C. (2000). Effective targeted gene 'knockdown' in zebrafish. Nat. Genet. *26*, 216–220.

Nornes, S., Mikkola, I., Krauss, S., Delghandi, M., Perander, M., and Johansen, T. (1996). Zebrafish Pax9 encodes two proteins with distinct C-terminal transactivating domains of different potency negatively regulated by adjacent N-terminal sequences. J. Biol. Chem. *271*, 26914–26923.

Nowak, M., Koster, C., and Hammerschmidt, M. (2005). Perp is required for tissue-specific cell survival during zebrafish development. Cell Death Differ. *12*, 52–64.

Okura, T., Gong, L., Kamitani, T., Wada, T., Okura, I., Wei, C. F., Chang, H. M., and Yeh, E. T. (1996). Protection against Fas/APO-1- and tumor necrosis factor-mediated cell death by a novel protein, sentrin. J. Immunol. *157*, 4277–4281.

Pichler, A., Gast, A., Seeler, J. S., Dejean, A., and Melchior, F. (2002). The nucleoporin RanBP2 has SUMO1 E3 ligase activity. Cell *108*, 109–120.

Piotrowski, T., and Nüsslein-Volhard, C. (2000). The endoderm plays an important role in patterning the segmented pharyngeal region in zebrafish (*Danio rerio*). Dev. Biol. *225*, 339–356.

Plaster, N., Sonntag, C., Busse, C. E., and Hammerschmidt, M. (2006). p53 deficiency rescues apoptosis and differentiation of multiple cell types in zebrafish flathead mutants deficient for zygotic DNA polymerase delta1. Cell Death Differ. *13*, 223–235.

Ross, S., Best, J. L., Zon, L. I., and Gill, G. (2002). SUMO-1 modification represses Sp3 transcriptional activation and modulates its subnuclear localization. Mol. Cell *10*, 831–842.

Rupp, R. A., Snider, L., and Weintraub, H. (1994). *Xenopus* embryos regulate the nuclear localization of XMyoD. Genes Dev. *8*, 1311–1323.

Ryu, S., Holzschuh, J., Erhardt, S., Ettl, A. K., and Driever, W. (2005). Depletion of minichromosome maintenance protein 5 in the zebrafish retina causes cell-cycle defect and apoptosis. Proc. Natl. Acad. Sci. USA *102*, 18467–18472.

Sachdev, S., Bruhn, L., Sieber, H., Pichler, A., Melchior, F., and Grosschedl, R. (2001). PIASy, a nuclear matrix-associated SUMO E3 ligase, represses LEF1 activity by sequestration into nuclear bodies. Genes Dev. *15*, 3088–3103.

Sapetschnig, A., Rischitor, G., Braun, H., Doll, A., Schergaut, M., Melchior, F., and Suske, G. (2002). Transcription factor Sp3 is silenced through SUMO modification by PIAS1. EMBO J. *21*, 5206–5215.

Schilling, T. F., and Kimmel, C. B. (1994). Segment and cell type lineage restrictions during pharyngeal arch development in the zebrafish embryo. Development *120*, 483–494.

Schilling, T. F., and Kimmel, C. B. (1997). Musculoskeletal patterning in the pharyngeal segments of the zebrafish embryo. Development *124*, 2945–2960.

Schmidt, D., and Muller, S. (2003). PIAS/SUMO: new partners in transcriptional regulation. Cell Mol. Life Sci. *60*, 2561–2574.

Seeler, J. S., and Dejean, A. (2003). Nuclear and unclear functions of SUMO. Nat. Rev. Mol. Cell Biol. *4*, 690–699.

Seufert, W., Futcher, B., and Jentsch, S. (1995). Role of a ubiquitin-conjugating enzyme in degradation of S- and M-phase cyclins. Nature *373*, 78–81.

Stelter, P., and Ulrich, H. D. (2003). Control of spontaneous and damage-induced mutagenesis by SUMO and ubiquitin conjugation. Nature *425*, 188–191.

Streisinger, G., Walker, C., Dower, N., Knauber, D., and Singer, F. (1981). Production of clones of homozygous diploid zebra fish (*Brachydanio rerio*). Nature *291*, 293–296.

Strunnikov, A. V., Aravind, L., and Koonin, E. V. (2001). *Saccharomyces cerevisiae* SMT4 encodes an evolutionarily conserved protease with a role in chromosome condensation regulation. Genetics. *158*, 95–107.

Tanaka, K., Nishide, J., Okazaki, K., Kato, H., Niwa, O., Nakagawa, T., Matsuda, H., Kawamukai, M., and Murakami, Y. (1999). Characterization of a fission yeast SUMO-1 homologue, pmt3p, required for multiple nuclear events, including the control of telomere length and chromosome segregation. Mol. Cell Biol. *19*, 8660–8672.

Taylor, K. M., and LaBonne, C. (2005). SoxE factors function equivalently during neural crest and inner ear development and their activity is regulated by SUMOylation. Dev. Cell *9*, 593–603.

Wada, N., Javidan, Y., Nelson, S., Carney, T. J., Kelsh, R. N., and Schilling, T. F. (2005). Hedgehog signaling is required for cranial neural crest morphogenesis and chondrogenesis at the midline in the zebrafish skull. Development *132*, 3977–3988.

Weiss, A., Herzig, A., Jacobs, H., and Lehner, C. F. (1998). Continuous Cyclin E expression inhibits progression through endoreduplication cycles in *Drosophila*. Curr. Biol. *8*, 239–242.

Weissman, A. M. (2001). Themes and variations on ubiquitylation. Nat. Rev. Mol. Cell Biol. *2*, 169–178.

Westerfield, M. (2000). The Zebrafish Book: A Guide for the Laboratory Use of Zebrafish, Eugene, OR: University of Oregon Press.

Yamaguchi, T., Sharma, P., Athanasiou, M., Kumar, A., Yamada, S., and Kuehn, M. R. (2005). Mutation of SENP1/SuPr-2 reveals an essential role for desumoylation in mouse development. Mol. Cell Biol. *25*, 5171–5182.

Yan, Y. L., *et al.* (2002). A zebrafish sox9 gene required for cartilage morphogenesis. Development *129*, 5065–5079.